



Research Article

Dielectric polarization and relaxation processes of the lithium-ion conducting PEO/PVDF blend matrix-based electrolytes: effect of TiO₂ nanofiller

Priyanka Dhatarwal¹ · R. J. Sengwa¹

Received: 18 January 2020 / Accepted: 30 March 2020 / Published online: 7 April 2020
© Springer Nature Switzerland AG 2020

Abstract

The effect of TiO₂ nanofiller concentration on the dielectric polarization and relaxation processes of (75PEO/25PVDF)/25 wt% LiClO₄-*x* wt% TiO₂ (*x*=0, 2, 5, 10, 15, and 20) compositions based nanocomposite solid polymer electrolyte (NSPE) films has been investigated by employing the dielectric relaxation spectroscopy. The SEM micrographs demonstrate that the dispersion of TiO₂ nanoparticles enormously alters the spherulitic morphology with the development of some cracks, pores, and wrinkles of these solution-cast prepared NSPE films. The X-ray diffraction study confirms that the heterostructures of these NSPE materials are semicrystalline and their degree of crystallinity increases irregularly with the increase of TiO₂ concentration, however the crystallinity of host polymer blend matrix of these electrolytes decreases. The complex dielectric permittivity spectra of these NSPE materials in the frequency range from 20 Hz to 1 MHz at 27 °C reveal that there is a dominant contribution of electrode polarization and interfacial polarization at lower frequencies, whereas the high frequency permittivity values attribute to dipolar and ionic polarizations. Four types of relaxation processes have been probed by the ‘master curve representation’ of the dielectric and electrical spectra of these solid ion–dipole complexes. It is observed that the addition of TiO₂ nanoparticles up to 10 wt% in these electrolytes influences the dielectric properties anomalously, but a huge decrease in the dielectric polarization and increase in the relaxation times are noted resulting in a significant decrease in the ionic conductivity of the film at 20 wt% TiO₂ concentration. The dependence of dc ionic conductivity of these lithium-ion conducting NSPE materials on the chain segmental relaxation time and also the degree of crystallinity has been explored. The results of these NSPE materials have also been compared with the TiO₂ nanoparticles loaded different polymer matrices and salts based electrolytes and discussed appropriately. These lithium-ion based electrolyte films are accredited for the solid-state ion-conducting energy storing devices from their electrochemical parameters characterized by LSV, CV, and CA techniques.

Keywords PEO/PVDF blend · Nanocomposite electrolytes · Dielectric relaxation · Ionic conductivity · SEM · XRD

1 Introduction

The solid polymer electrolytes (SPEs) have attracted huge attention in the last four decades and now matured enough owing to their tremendous technological importance established in the development of flexible-type all-solid-state advanced ion-conducting devices (i.e.,

rechargeable batteries, fuel cells, supercapacitors, solar cells, sensors, and so forth) [1–10]. These materials are novel and advantageous over their liquid counterparts especially relevant to the battery applications because they have adequate ionic conductivity and numerous other fascinating features like wide operating temperature range, lightweight, good shelf life, high energy density,

✉ Priyanka Dhatarwal, dhatarwalpriyanka@gmail.com; ✉ R. J. Sengwa, rjsengwa@rediffmail.com; rjs.ph@jnvu.edu.in | ¹Dielectric Research Laboratory, Department of Physics, Jai Narain Vyas University, Jodhpur 342 005, India.



leakage-free, ease of preparation, the flexibility of miniaturization, reduced flammability, low toxicity, good stability during the charge–discharge cycles, as well as appreciable mechanical and thermal stabilities [2, 4, 8–10]. So far, a variety of SPEs including nanocomposite SPEs (NSPEs), plasticized SPEs (PSPEs), and plasticized nanocomposite SPEs (PNSPEs) have been beautifully developed with state-of-the-art, and their technological significance has been greatly appreciated with breakthroughs in the energy storing devices (batteries and supercapacitors) [2, 3, 6–8, 10, 11]. At the early stage of the development of solid-state electrolyte materials, they exhibited some drawbacks from the technology point of view and therefore tremendous efforts have been made in the last decade researches to overcome the drawbacks and are thoroughly addressed in several recent reviews [1–12].

Many approaches such as the use of polymer blends as promising host matrices [13–19], inclusion of inorganic and organic nanofillers for improving thermal, mechanical, and ion transportation properties [20–23], the addition of various ionic liquid and/or dipolar liquid plasticizers for increasing degree of salt dissociation and reducing the crystallinity of polymer matrix [24–27], and consideration of different preparation methods suitable from the industrial point of view [28–33]. Furthermore, some combinations of these different approaches have also been taken into consideration for exploiting different kinds of SPE materials with a variety of appealing properties [17, 20, 26, 34]. Among these approaches, the blending of polymers and their use as host matrices for the preparation of appropriate properties SPEs is a valid and more feasible green chemistry process that has been exemplified by various research groups [10, 17–21, 26, 29, 32]. The blending process not only suppresses the unwanted properties of individual polymers but also enhances the required superior properties that can be engineered through an appropriate compositional weight ratio of the blended polymers [14, 17, 18, 35, 36]. The addition of nano-sized fillers in the host polymer matrix is also a widely popular and efficient strategy to get improved physicochemical properties of the prepared NSPE materials [6, 10, 18, 22, 30, 37]. It has been observed that the nanofiller increases free volume in the polymeric composite material and creates additional favourable ion conductive paths due to which ions mobility increases [5, 10]. Further, numerous studies have also validated the fact that the nanofillers decrease the crystalline content of the semicrystalline polymer matrix and thereby make it more fascinating ion-conductive amorphous host medium [22, 23, 37].

For the preparation of SPE films, the poly (ethylene oxide) (PEO) is extensively used as a host polymer matrix since the development of first-ever SPE material [5, 8, 10], and it is still the prime choice of researchers for progressive

work on the ion-conducting flexible-type SPE materials [38–41]. The key favorable properties of the PEO in regards to its use as SPE materials are its easy processing and high solvating power for the alkali metal salts [5, 8, 10]. Although the degree of crystallinity of the PEO matrix (~ 73.6%) is high [42], its relatively fast chain segmental motion facilitates the hopping mechanism of ions transportation [33]. However, poor thermal and mechanical properties of the PEO matrix-based SPEs are major drawbacks in regard to device workability at higher temperatures [5, 10]. Therefore, the blends of PEO with several polymers of better thermophysical properties are largely considered for the preparation of promising SPE, NSPE, PSPE, and PNSPE materials [14, 17–21, 26, 31, 32, 36, 43]. The semicrystalline polar poly(vinylidene fluoride) (PVDF) matrix has relatively appreciable physicochemical and electroactive properties [44] and therefore it is considered in several researches for the development of advanced SPE materials [45–47]. Numerous studies on the blend matrices of PEO/PVDF have realized some favourable properties in regards to their suitability as a host matrix for the SPEs and therefore this polymer blend matrix is used for the preparation of a variety of SPEs [13–15, 35, 36, 48] and also electrolyte membranes [16, 49, 50] suitable for all-solid-state ion-conducting devices. A survey of literature confirms that for the lithium-ion conducting SPE materials, the LiClO_4 is one of the appealing ionic dopants used enormously for the preparation of SPEs [10, 23, 27, 33, 36]. The investigations on numerous NSPE materials have claimed that the dispersion of TiO_2 nanoparticles mostly increases the ionic conductivity, and some studies also reported an unexpected increase by a few orders of magnitude [22, 23, 30, 49–62]. Some studies have concluded that only the acidic groups surface-modified TiO_2 and some other inorganic nanofillers are effective in increasing the conductivity of the NSPE materials [63, 64]. The molecular simulation studies established that the nanoparticles slow down the dynamics of polymer chain segments near their surface due to which mobility of ions reduces and thereby the ionic conductivity of the polymer electrolytes decreases in presence of a nanofiller [65, 66]. Additionally, the study of TiO_2 based NSPEs is not only interesting for the development of energy storage devices point of view but also highly appreciable in regards to energy harvesting devices [49, 67].

Recently, we investigated detailed structural and dielectric properties of the PEO/PVDF blends over the entire blend composition range [42], these polymers blends based nanocomposites [68], and also a variety of SPE materials [35, 69, 70]. In continuation of these researches on the PEO/PVDF blend matrix-based various types of flexible dielectric and electrolyte materials, the present manuscript deals with the NSPE materials comprising

(75PEO/25PVDF)/25 wt% LiClO₄-*x* wt% TiO₂ compositions. The manifold aims of this work are; first, to study and report the detailed morphological, structural, dielectric polarization and relaxations, and also ion conduction behaviour of these NSPE materials with the variation of TiO₂ nanofiller concentration, second, to explore the effect of TiO₂ concentration on the various relaxation times and their correlation with the ion transport mechanism in these heterogeneous ion-dipole complexes, and third, to confirm how much this wide bandgap semiconductor inorganic TiO₂ nanofiller is effective in the improvement of the promising properties of PEO/PVDF blend matrix-based electrolyte materials.

2 Experimental

2.1 Materials

The Sigma-Aldrich PEO of $M_v = 600,000 \text{ g mol}^{-1}$ (CAS No. 25322-68-3), PVDF of $M_w \sim 534,000 \text{ g mol}^{-1}$ (CAS No. 24937-79-9), LiClO₄ of battery grade (CAS No. 7791-03-9), and TiO₂ of particle sizes less than 21 nm (CAS No. 13463-67-7) were used as primary materials for the preparation of the NSPE films. *N,N*-dimethyl formamide (DMF) (CAS No. 68-12-2) of Loba Chemie, India was used as the solvent.

2.2 Preparation of NSPE films

The NSPE films (i.e., (75PEO/25PVDF)/25 wt% LiClO₄-*x* wt% TiO₂) of varying TiO₂ concentrations (*x*=0, 2, 5, 10, 15, and 20 wt% designated respectively as NSPE0 (i.e., SPE), NSPE2, NSPE5, NSPE10, NSPE15, and NSPE20) were obtained by casting from solution. Firstly, six polymeric solutions for PEO/PVDF blend of compositional weight ratio 75/25 wt/wt% were prepared by taking the amounts of PEO (0.75 g) and PVDF (0.25 g) in stoppered conical glass flasks for each sample, and dissolving them in DMF (15 ml) at 80 °C with magnetic stirring. Thereafter, 25 wt% amount of LiClO₄ (0.25 g) with respect to the amount of polymer blend (1 g) was added to each polymeric solution and then these were again subjected to magnetic stirring for dissolution of the salt completely which resulted primary polymeric electrolyte solutions ((75PEO/25PVDF)/25 wt% LiClO₄). Thereafter, the required amounts of TiO₂ for its 2 (0.02 g), 5 (0.05 g), 10 (0.10 g), 15 (0.15 g), and 20 (0.20 g) wt% concentrations with respect to the amount of polymer blend (1 g) were dispersed in DMF and then added in respective five samples of the primary polymeric electrolyte solutions. These solutions were again stirred magnetically for 2 h to achieve good dispersibility of TiO₂ nanoparticles in the electrolyte solutions. Finally, these five heterogeneous polymeric electrolyte solutions of different TiO₂ concentrations and

one sample of primary polymeric electrolyte solution were casted on to glass petri dishes. For the film formation, the casted solutions were heated at 70 °C on a thermostated hot plate until the solvent evaporation was completed. These were then cooled down to room temperature which resulted free-standing NSPE films. All these films were vacuum dried at 40 °C for a day to remove solvent traces and then were stored in the desiccator.

2.3 Measurements

The micro-images of NSPE0, NSPE5, and NSPE10 films and their EDX spectra were recorded by employing a scanning electron microscope (SEM; Carl ZEISS EVO MA15) equipped with energy dispersive X-ray (EDX) analyzer which run at EHT voltage of 15 kV. The XRD patterns of all these NSPE films were collected in reflection mode using the PANalytical X'pert Pro multipurpose powder diffractometer operated at 45 kV and 40 mA. The frequency dependent electrical measurements of each NSPE film sandwiched between the electrodes of dielectric test fixture were performed using Agilent Technologies 4284A precision LCR meter and 16451B solid dielectric test fixture. These measurements were carried out at 1-V electric signal of frequency range 20 Hz–1 MHz, at 27 °C. The measured values of frequency dependent electrical quantities (i.e., capacitance C_p , resistance R_p , and dissipation factor D ($\tan\delta$)) were used for the determination of complex dielectric permittivity, electrical conductivity, impedance, and electric modulus spectra of the NSPE films from the respective relations described elsewhere [70]. The electrochemical analyzer (CH Instruments, Inc. CHI 608E) was employed for carrying out the linear sweep voltammetry (LSV), cyclic voltammetry (CV), and chronoamperometry (CA) of the NSPE films. A symmetrical cell for each film sandwiched between the stainless steel (SS) blocking electrodes was constructed for collecting LSV, CV, and CA traces following the procedure explained in the previous publication [71].

3 Results and discussion

3.1 SEM images and microstructures

Figure 1 presents the digital pictures, SEM images, and EDX spectra of NSPE0, NSPE5, and NSPE10 films as representative samples. It can be noted from the digital pictures that the NSPE0 film has some transparency but the TiO₂ dispersed films are opaque and milky. The manual bending, twisting, and touching operations realize that the NSPE0 film is little sticky and relatively more flexible whereas the stickiness and flexibility of the NSPE films reduce with the increase of TiO₂ concentration. These manual observations

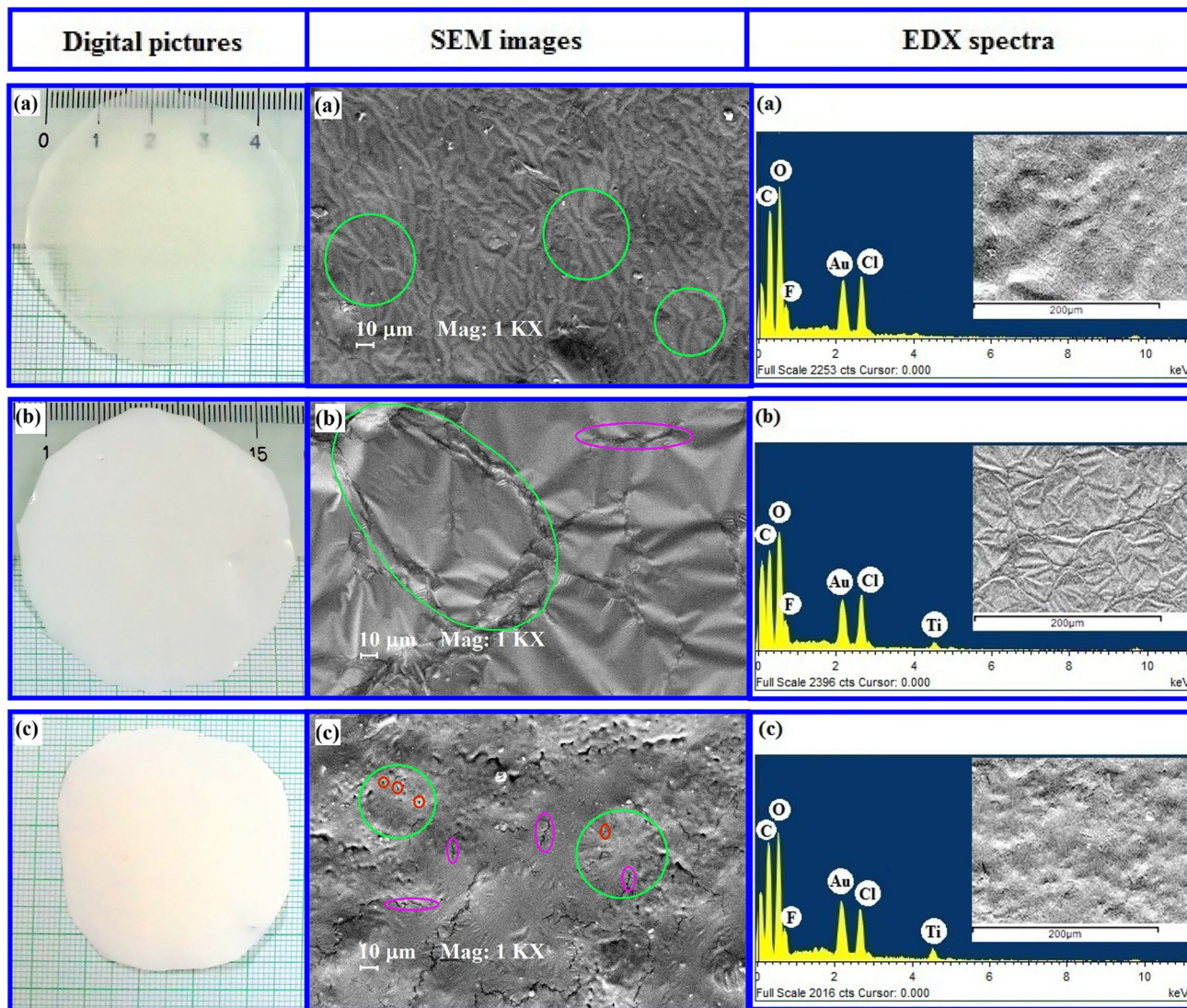


Fig. 1 The digital pictures, SEM images, and EDX spectra of (75PEO/25PVDF)/25 wt% LiClO_4 -x wt% TiO_2 films; **a** NSPE0 ($x=0$) with encircled spherulites, **b** NSPE5 ($x=5$) with typical cracked

earth texture encircled by ellipses, and **c** NSPE10 ($x=10$) with encircled spherulites, and cracks and pores encircled by ellipses of different colors

infer that the TiO_2 loading increases the mechanical strength of the NSPE films which are in agreement with earlier experimental results on the TiO_2 containing other NSPE films [57, 58, 62].

The micrograph of NSPE0 film (Fig. 1a) shows that there are macro-sized spherulites (some are encircled) which represent the crystallites of PEO blended with PVDF [42], although, the pristine PEO and PVDF films exhibit highly distinguishable spherulites surrounded by the amorphous amount of these polymers [14, 42, 72]. The interconnected spherulites of the NSPE0 film evidence cross-linked chain structures of the blended polymers through ion-dipole complexes due to which a large amount of these polymers crystals turn into amorphous content. Further, the

wrinkles or fibril-like textures exhibited over the entire surface evidence large inner forces acting in these heteromaterials during the process of film formation as reported for a similar type of electrolyte materials [17]. Figure 1b reveals that 5 wt% amount of TiO_2 dispersed NSPE5 film exhibits highly different microstructures as compared to that of the NSPE0 film. Typical dry cracked earth texture with fluffier and crumpled structures can be seen in the micrograph of NSPE5 film. Further, when the TiO_2 amount is increased up to 10 wt%, then the NSPE10 film texture (Fig. 1c) turned rougher having several cracks with typical micro-sized pores. Some macro-size spherulitic features of typical granular shapes have also appeared which indicate strong electrostatic interaction of TiO_2 nanoparticles with

the polymer structures. This SEM image also infers that the TiO₂ nanoparticles exist almost homogeneously dispersed in the prepared film.

The EDX spectrum of NSPE0 film (Fig. 1a) confirms that there is the presence of only its constituent elements which is evidence of the purity of film. This film has energy peaks of carbon (C) (at 0.28 keV), oxygen (O) (at 0.53 keV), fluorine (F) (at 0.68 keV), and chlorine (Cl) (at 2.62 keV) which are according to its composition. In addition to these peaks, the EDX spectra of NSPE5 (Fig. 1b) and NSPE10 (Fig. 1c) films also exhibit the peak of titanium (Ti) (at 4.51 keV) and its intensity is found high for the NSPE10 film as compared to that of the NSPE5 film, which is expected according to the increase in the concentration of TiO₂ nanofiller. Further, the gold (Au) peak observed at 2.15 keV in the EDX spectra of all these films is due to the use of this element for sputtering over the surfaces of the films prior to their EDX mapping.

3.2 XRD spectra and crystal structures

The XRD patterns in 2θ range from 10° to 50° of the (75PEO/25PVDF)/25 wt% LiClO₄- x wt% TiO₂ films are depicted in Fig. 2. These patterns have moderate intensities peaks of the PEO, PVDF, and TiO₂ representing their crystalline content (marked in the figure), and also a huge background hump in each pattern attributing to amorphous content. These patterns confirm that these semicrystalline films are predominantly amorphous. The assignments of main crystalline peaks with their positions 2θ , reflection plane indices (hkl), and the determined values of basal spacing d , full width at half maximum (FWHM) β , crystallite size L , and intensity I for all these NSPE films are listed in Table 1.

The NSPE0 (primary SPE without nanofiller) film displays the characteristic peaks of PEO (19.11° and 23.38°) but their intensities are much lower than that of the pristine PEO film [33] revealing that a large amount of PEO crystallites have turned into amorphous content due to formation of ion-dipole complexes. A significant intensity β -phase (20.53°), a very low intensity γ -phase (22.02°), and also α -phase (36.32°) crystals peaks in the XRD pattern of this film confirms the PVDF polymorphism [15, 42, 44, 62]. Further, as compared to peaks intensities and positions of NSPE0 film, it is found that there is an increase in intensities of the PEO and PVDF peaks with a small change in their positions for the NSPE2 film (see 2θ and I values given in Table 1). Furthermore, a low intensity peak at 25.17° (101) is also exhibited in the XRD pattern of this film which is the main characteristic peak of tetragonal anatase TiO₂ [73]. Besides this peak, several weak intensity peaks around 27°, 36.08°, 37.75°, and 47.92° can be noted with increasing TiO₂ contents in the films attributing to

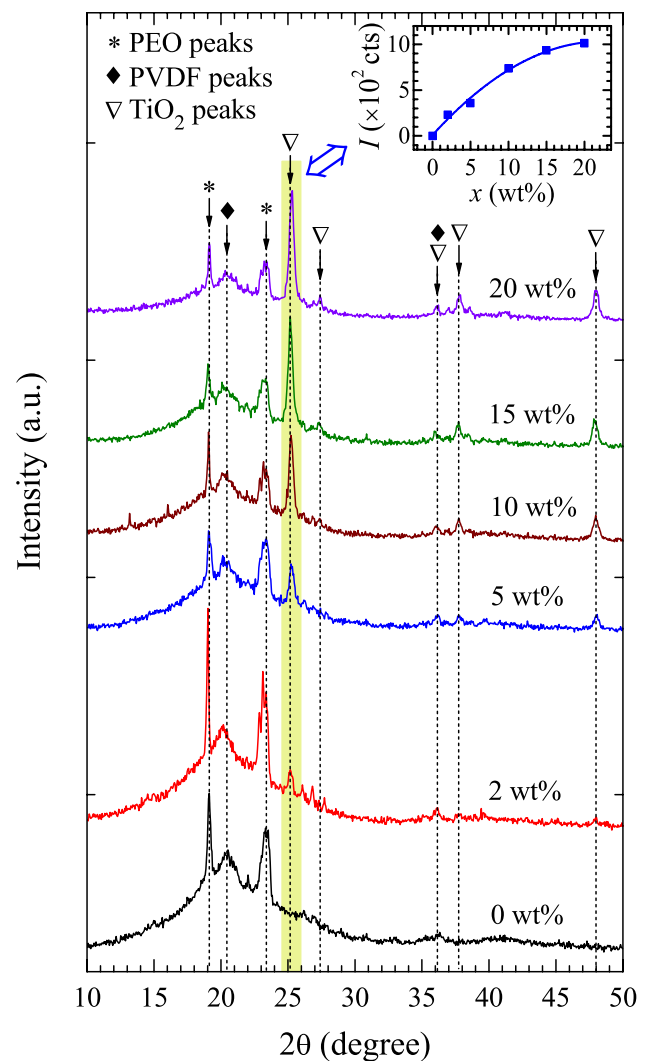


Fig. 2 The XRD patterns of (75PEO/25PVDF)/25 wt% LiClO₄- x wt% TiO₂ films ($x=0, 2, 5, 10, 15,$ and 20) marked with PEO, PVDF, and TiO₂ peaks and the characteristic TiO₂ peak highlighted with a coloured background. The plot of intensity I versus x (wt%) for the characteristic intense peak of TiO₂ at $\sim 25^\circ$ (101) of these NSPE films is shown in the inset

anatase and rutile phases of TiO₂ [73]. It is also observed from these XRD patterns that with the increase of TiO₂ concentrations up to 20 wt%, the peaks intensities of both the polymers decrease anomalously, whereas there is a gradual increase in the intensities of TiO₂ peaks. The main characteristic peak of TiO₂ is highlighted with a coloured background in Fig. 2 for these NSPE films. The inset of this figure shows the plot of TiO₂ peak intensity versus x (wt%) which increases non-linearly with the increase of TiO₂ content in these NSPE films. This finding evidence that the nanoparticles incorporated in these electrolyte films are uniformly distributed over the entire volume of each NSPE film. Further, the major crystallite peaks of pristine

Table 1 Values of 2θ , d , β , L , and I corresponding to various diffraction peaks of (75PEO/25PVDF)/25 wt% LiClO₄- x wt% TiO₂ films

Diffraction peaks	2θ (degree)	d (nm)	β ($\times 10^{-3}$ rad)	L (nm)	I (counts)
(75PEO/25PVDF)/25 wt% LiClO ₄ film (NSPE0)					
PEO (120)	19.11	0.464	4.59	31.99	778
β PVDF (110),(200)	20.53	0.432	17.65	8.34	263
γ PVDF (020)	22.02	0.403	2.50	59.11	123
PEO (112),(032)	23.38	0.380	13.11	11.28	640
α PVDF (200)	36.32	0.247	10.90	13.97	65
(75PEO/25PVDF)/25 wt% LiClO ₄ -2 wt% TiO ₂ film (NSPE2)					
PEO (120)	19.02	0.466	2.89	49.20	1208
β PVDF (110),(200)	20.14	0.440	16.63	8.84	282
PEO (112),(032)	23.14	0.384	12.28	12.03	890
TiO ₂ (101)	25.17	0.353	6.99	21.20	230
(75PEO/25PVDF)/25 wt% LiClO ₄ -5 wt% TiO ₂ film (NSPE5)					
PEO (120)	19.09	0.465	5.67	25.89	470
β PVDF (110),(200)	20.17	0.440	17.08	8.61	193
PEO (112),(032)	23.32	0.381	13.98	10.58	508
TiO ₂ (101)	25.26	0.352	7.33	20.25	358
(75PEO/25PVDF)/25 wt% LiClO ₄ -10 wt% TiO ₂ film (NSPE10)					
PEO (120)	19.07	0.465	3.07	47.80	498
β PVDF (110),(200)	20.46	0.434	16.93	8.69	200
PEO (112),(032)	23.18	0.383	9.29	15.92	376
TiO ₂ (101)	25.24	0.353	6.98	21.26	738
(75PEO/25PVDF)/25 wt% LiClO ₄ -15 wt% TiO ₂ film (NSPE15)					
PEO (120)	19.03	0.466	5.39	27.23	375
β PVDF (110),(200)	20.12	0.441	20.75	7.09	184
PEO (112),(032)	23.24	0.382	13.44	11.00	356
TiO ₂ (101)	25.19	0.353	7.14	20.79	935
(75PEO/25PVDF)/25 wt% LiClO ₄ -20 wt% TiO ₂ film (NSPE20)					
PEO (120)	19.13	0.464	3.12	47.00	418
β PVDF (110),(200)	20.35	0.436	22.75	6.46	143
PEO (112),(032)	23.46	0.379	12.93	11.44	291
TiO ₂ (101)	25.29	0.352	7.10	20.89	1013

LiClO₄ (21.02° and 23.04°) [74] are not exhibited in these XRD patterns which confirms the complete dissolution of the added amount of salt in the prepared NSPE materials.

The degree of crystallinity X_c of the electrolyte films (i.e., $X_{c(p)}$ of the host polymer matrix and $X_{c(t)}$ of the total bulk

composite material) were determined from the areas of crystalline and amorphous parts in XRD patterns using the area-based relation given in the literature [42, 68]. It can be noted from Table 2 that the $X_{c(p)}$ values of TiO₂ dispersed NSPE films are significantly lower whereas $X_{c(t)}$ values are

Table 2 Values of degree of crystallinity $X_{c(p)}$ (%) and $X_{c(t)}$ (%), various relaxation times τ_{EDL} , τ_{MWS} , τ_s , and τ_σ , dc ionic conductivity σ_{dc} ($\sigma_{dc(\sigma)}$ and $\sigma_{dc(Rb)}$), fractional exponent n , and total ion transference

number t_{ion} of (75PEO/25PVDF)/25 wt% LiClO₄- x wt% TiO₂ films for $x=0, 2, 5, 10, 15$, and 20

NSPE films	$X_{c(p)}$ (%)	$X_{c(t)}$ (%)	τ_{EDL} ($\times 10^{-4}$ s)	τ_{MWS} ($\times 10^{-5}$ s)	τ_s ($\times 10^{-6}$ s)	τ_σ ($\times 10^{-7}$ s)	$\sigma_{dc(\sigma)}$ (μ S/cm)	$\sigma_{dc(Rb)}$ (μ S/cm)	n	t_{ion}
NSPE0	22.9	22.9	5.31	2.10	1.69	1.34	3.25	5.3	0.50	0.990
NSPE2	17.5	24.2	10.62	3.46	3.09	3.08	2.40	3.8	0.73	0.938
NSPE5	15.4	24.7	8.80	2.45	1.96	1.71	2.60	4.5	0.57	0.970
NSPE10	17.3	26.4	13.05	2.97	1.89	1.54	2.95	4.6	0.72	0.941
NSPE15	16.8	34.9	3.55	1.72	1.74	2.08	2.42	4.0	0.62	0.976
NSPE20	13.0	37.0	5.94	3.31	5.89	12.92	0.47	0.8	0.68	0.931

higher as compared to that of the NSPE0 (SPE film without nanofiller). Further, these X_c values anomalously vary with the increase of TiO_2 concentration in the NSPE films. The effect of $X_{c(p)}$ and $X_{c(t)}$ values on the ionic conductivity of these NSPE films is considered in the later section of this manuscript.

3.3 Dielectric spectra and polarization processes

Figure 3 presents the complex dielectric permittivity (real part ϵ' and imaginary part ϵ'') and dielectric loss tangent ($\tan\delta = \epsilon''/\epsilon'$) values as a function of frequency for the (75PEO/25PVDF)/25wt% LiClO_4 - x wt% TiO_2 films, at 27

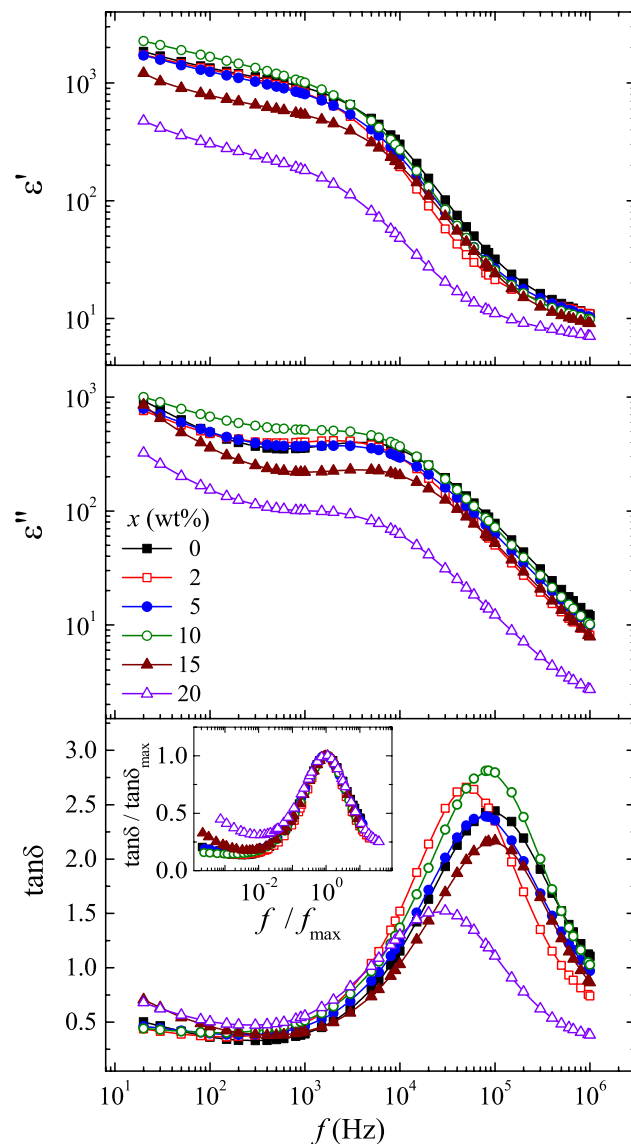


Fig. 3 The spectra of complex dielectric permittivity (real part ϵ' and imaginary part ϵ'') and dielectric loss tangent $\tan\delta$ of (75PEO/25PVDF)/25 wt% LiClO_4 - x wt% TiO_2 films ($x=0, 2, 5, 10, 15,$ and 20), at 27 °C. Inset shows the scaled plots of $\tan\delta$ spectra

°C. It can be noted that the respective shapes of these spectra of ϵ' , ϵ'' , and $\tan\delta$ for all the NSPE films are almost identical. Further, at a fixed frequency, there are relatively small changes in ϵ' and ϵ'' values with the increase of TiO_2 concentration up to 10 wt%, but a noticeable decrease at 15 wt% in the lower frequency range and a huge decrease at 20 wt% over the entire frequency range is observed. These results verify that there is a moderate alteration in the overall amount of ion–dipole ordering in the presence of TiO_2 nanoparticles up to 10 wt% but a large disordering is exhibited for the higher concentration of the nanofiller. The magnitude and dispersion trend of frequency dependent ϵ' and ϵ'' values for these films evidence the existence of four types of dielectric polarization processes in the frequency range from 20 Hz–1 MHz which are demonstrated for some other electrolyte materials in recent publications [69, 70]. The dominance of the electrode polarization (EP) process is exhibited at lower frequencies as evident from the high dielectric permittivity values of about three orders of magnitude for these NSPE films. Further, at intermediate frequencies, there is a significant contribution of interfacial polarization (IP) process in these heterogeneous materials due to which there is a slow decrease in ϵ' values and ϵ'' values resulting a hump in the frequency range from 1 kHz–10 kHz. A huge dispersion of ϵ' and ϵ'' values at higher frequencies can be attributed, firstly to the molecular polarization and then the ionic polarization with increasing frequency. The probing of relaxations corresponding to these processes is executed with the help of 'master curve representation' in the later section.

The $\tan\delta$ spectra of these NSPE materials characteristically exhibit the intense relaxation peaks in the high frequency region which are corresponding to the ions coupled chain segmental motion. It can be noted that the intensities and positions of the $\tan\delta$ peaks anomalously change with the increase of TiO_2 concentration in these NSPE films which reveals that the heterogeneous ion–dipole–nanoparticle interactions vary irregularly and hence the dielectric properties of these materials cannot be tuned by changing TiO_2 concentration. The scaled plots of $\tan\delta$ spectra (i.e. $\tan\delta/\tan\delta_{\max}$ versus f/f_{\max}) shown in the inset of the figure for these NSPE materials are found reasonably overlapped (except NSPE20 film at lower frequencies) which manifests that they have a similar trend of the distribution of their main relaxation time [69]. The deviation at lower frequencies evidences a significant difference in electrode polarization behaviour of these NSPE materials of nanofiller concentration > 10 wt%.

3.4 Conductivity spectra and charge transportation

Figure 4 demonstrates the ac electrical conductivity (real part σ') spectra of the NSPE films at 27 °C, which exhibit

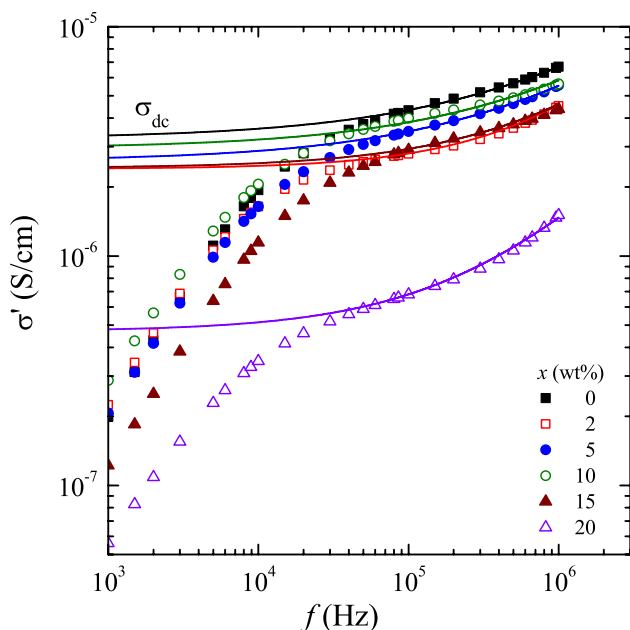


Fig. 4 The spectra of real part σ' of ac electrical conductivity for (75PEO/25PVDF)/25 wt% LiClO_4 - x wt% TiO_2 films ($x=0, 2, 5, 10, 15,$ and 20), at 27°C . Solid lines on these σ' spectra are the power law fit $\sigma'(\omega) = \sigma_{\text{dc}} + A\omega^n$ of high frequency experimental data

all the characteristic dispersion regions similar to those demonstrated for other electrolyte materials investigated earlier [19, 20, 31–34, 43, 53, 69, 70]. In the low frequency region, the σ' values increase sharply with the increase of frequency owing to the fast suppression of the electric double layer (EDL) capacitances which are relatively large at the initial frequency of the spectra. After full suppression of the EDLs, these spectra firstly exhibit a very narrow range of dc plateau and then show dc to ac transition of the charge carriers according to Jonscher power law relation $\sigma'(\omega) = \sigma_{\text{dc}} + A\omega^n$. The power law fits of high frequency σ' data points are shown by solid lines on the spectra in the figure, and the observed values of fit parameters i.e., dc ionic conductivity σ_{dc} (denoted as $\sigma_{\text{dc}(\sigma')}$) and fractional exponent n of these NSPE films are listed in Table 2. The σ_{dc} values are found of the order of 10^{-6} S/cm for these NSPE films which show a small variation with the increase of TiO_2 concentration up to 15 wt%. The σ_{dc} value of 20 wt% TiO_2 containing NSPE20 film is found about one order of magnitude lower in comparison to the other low concentration TiO_2 containing NSPE films (see Table 2). Further, it can be noted that the σ_{dc} values of all the TiO_2 containing NSPE films are lower than that of the NSPE0 film without nano-filler. This finding confirms that the dispersion of TiO_2 nanoparticles in the primary composition of these electrolytes is not effective in regards to enhancing the ion transport mechanism. Further, the n values of these NSPE materials are found in the range 0.50 to 0.73, which are much

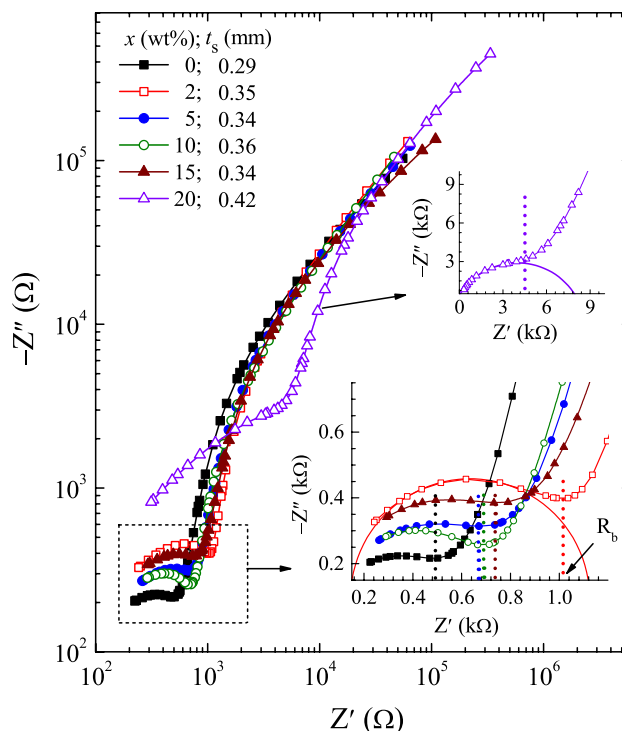


Fig. 5 Complex impedance plane plots (Z'' versus Z') for (75PEO/25PVDF)/25 wt% LiClO_4 - x wt% TiO_2 films ($x=0, 2, 5, 10, 15,$ and 20) of thicknesses t_s (mm), at 27°C . Insets show the enlarged view of high frequencies on the linear scale and bulk resistances R_b marked with vertical dashed lines, and semicircle drawn with high frequency data for the NSPE2 ($x=2$) and NSPE20 ($x=20$) films

lower than unity confirming that the ion transportation takes place predominantly through hopping mechanism and this fact agrees with the results on several other SPE materials investigated with dielectric spectroscopy [20, 21, 29, 31–33, 70].

3.5 Complex impedance plots

The Nyquist plots of frequency dependent complex impedance data (Z'' versus Z') on the logarithmic scale for the NSPE films at 27°C are given in Fig. 5. All these complex plane plots exhibit two characteristic parts of the electrolyte films; (i) the tilted large spikes formed by low frequency data representing the EDL capacitances, and (ii) the small sized arcs formed by the high frequency data (enlarged view on the linear scale shown in insets of the figure which are parts of semicircle drawn for some representative samples) attributing to bulk properties of the electrolyte materials. Each arc represents the equivalent parallel combination circuit of an energy storing element C_p and a dissipating element R_p . The shapes of these impedance plots are found in good resemblance with that of the several similar types of electrolyte

materials based on different polymer matrices [14, 26, 30, 32, 35, 43, 69]. Further, the shape of the Nyquist plot of NSPE20 film indicates that the arc and spike parts in the plot are not clearly separable as usually noted for the other electrolytes which reflect that there may be few stiffer domains on the film surfaces resulting in poor electrode/electrolyte contact [70].

The bulk resistance R_b which is the dc resistance of the electrolyte material was noted from the real axis Z' for each film at which the arc and spike intersect as marked by vertical dashed lines in the figure. Taking these R_b values and the film thicknesses t_s marked in Fig. 5, the dc ionic conductivities were determined by the relation $\sigma_{dc} = t_s/R_b \cdot A$ where $A = 11.35 \text{ cm}^2$ is the active electrode surface area of the test fixture. The observed σ_{dc} (denoted by $\sigma_{dc(Rb)}$) values for these films from this R_b based relation are also listed in Table 2. It can be noted from this table that the $\sigma_{dc(Rb)}$ and $\sigma_{dc(\sigma')}$ values for each sample are of the same order of magnitude which validates the suitability of both the methods used for determination of ionic conductivity of the solid polymer electrolytes. Some differences may be there in the $\sigma_{dc(\sigma')}$ and $\sigma_{dc(Rb)}$ values of the ion-conducting electrolytes because of possible error in the estimated R_b values from the complex impedance plots as explained earlier [20, 32, 39, 69–71].

3.6 Electric modulus spectra

The complex electric modulus (real part M' and imaginary part M'') spectra for the NSPE materials at 27 °C are depicted in Fig. 6. These spectra on semi-logarithmic scale reveal that the low frequency range in which the M' and M'' values are about zero represents the EP dominated region, whereas the steep rise in the high frequency range attributes to bulk properties of the electrolyte materials which are common characteristics reported for several electrolyte materials [18–21, 35, 69, 70]. The M'' spectrum of the NSPE20 film exhibits a peak at about 200 kHz corresponding to the conductivity relaxation process at which the long range motion of charge carriers turn to localized hopping mechanism [26, 32, 33, 71, 75]. The shape of M'' spectra for the NSPE films containing TiO_2 concentration $0 \leq x \leq 15$ reflects that conductivity relaxation process peaks of these materials are just above 1 MHz confirming their relatively fast hopping mechanism as compared to that of the NSPE20 film. The Nyquist plot (M'' versus M') of the NSPE5 film as a representative is shown in the inset of the figure which confirms the Cole–Cole dispersion of its conductivity relaxation process, and the same is true for the other NSPE materials.

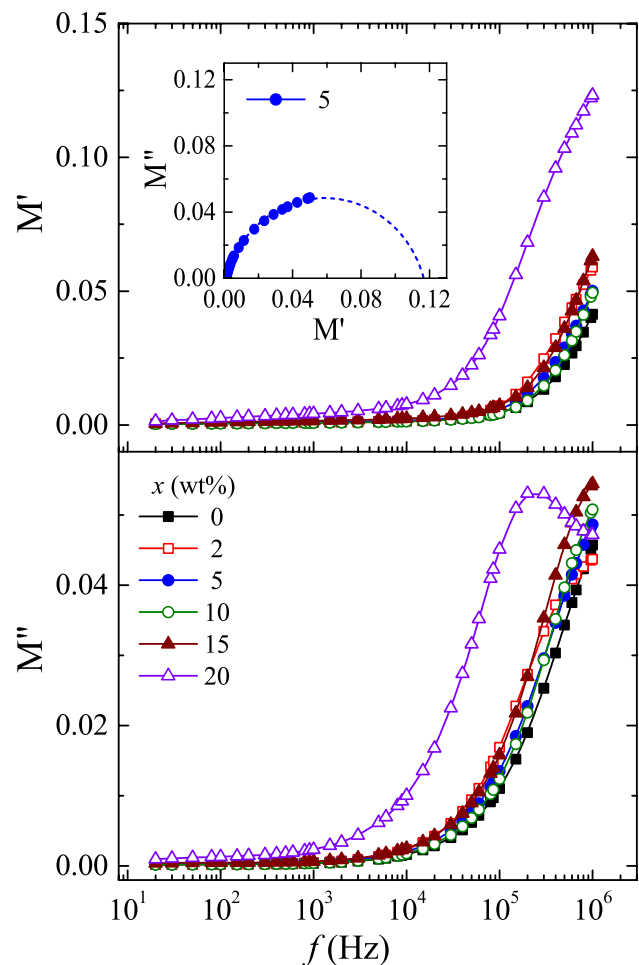


Fig. 6 The electric modulus spectra (real part M' and imaginary part M'') of (75PEO/25PVDF)/25 wt% LiClO_4 - x wt% TiO_2 films ($x=0, 2, 5, 10, 15,$ and 20), at 27 °C. Inset shows the Cole–Cole plot for the NSPE5 ($x=5$) film

3.7 Confirmation of relaxation processes

Figure 7 shows a novel procedure of probing different relaxation processes in the heterogeneous electrolytes by 'master curve representation' of all the dielectric and electric functions which is explained in the recent publications [69, 70, 75]. This figure shows the spectra of dielectric and electric functions drawn on the same frequency scale for NSPE2 (Fig. 7a) and NSPE20 (Fig. 7b) films as representatives of these materials. The frequencies corresponding to four different relaxation processes occurring in the frequency range from 20 Hz to 1 MHz are marked by vertical dashed lines in this figure. These relaxation processes denoted by the frequencies f_{EDL} , f_{MWS} , f_{sr} and f_{σ} in the figure are corresponding to the charging and discharging of EDL capacitances, charge dynamics of the MWS mechanism with a significant contribution of the EDLs relaxation, ions coupled chain segmental motion, and the ionic

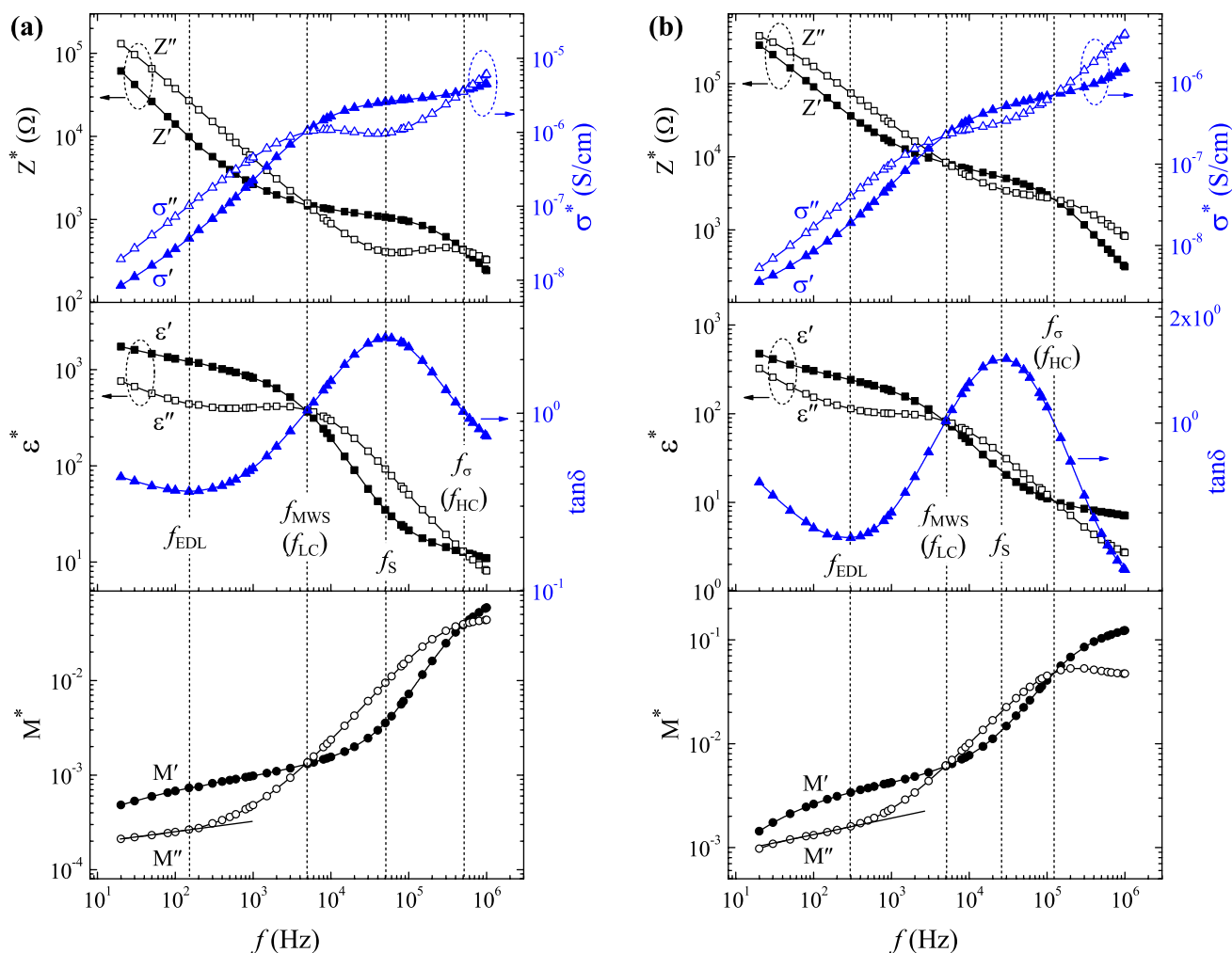


Fig. 7 ‘Master curve representation’ of various dielectric and electrical functions for (75PEO/25PVDF)/25wt% LiClO_{4-x} wt% TiO₂ films; **a** NSPE2 (*x*=2) and **b** NSPE20 (*x*=20) at 27 °C. The relaxation fre-

quency corresponding to different relaxation processes are marked with vertical dashed lines

conductivity relaxation, respectively. The detailed identification procedure of these relaxation processes for the complex SPE materials is demonstrated in our recent publications [70].

For these NSPE films, the lower cross-frequency f_{LC} and the higher cross-frequency f_{HC} of the real and imaginary parts of the dielectric and electric functions can be assigned to the MWS and conductivity relaxation processes, respectively. For non-Debye type ac electrical conductivity dispersion of the electrolyte materials, the conductivity relaxation frequency f_{σ} appears at a little higher value than the f_{HC} , but the trend of variation of f_{σ} with the change in the composition of the electrolytes seems to remain same as that noted in the f_{HC} values. Further, the frequency corresponding to the minimum of $\tan\delta$ and ϵ'' in the lower frequency region where M''

also starts to deviate from linearity can be labeled to EDL relaxation process. The frequency corresponding to the peak in $\tan\delta$ spectra where Z'' and σ'' also exhibit minimum can be labeled to the ions coupled chain segmental relaxation process. The values of relaxation times for these processes i.e., τ_{EDL} , τ_{MWS} , τ_s , and τ_{σ} are evaluated from the respective relaxation frequencies using the relation $\tau = 1/2\pi f$ and the observed values for these materials are listed in Table 2. The anomalous variation in these relaxation times with the increase of TiO₂ concentration in these NSPE films is noted. These results confirm that the heterogeneous polymeric electrolyte films at ambient temperature, in general, might exhibit all four different relaxation processes when they are characterized by the DRS technique with six orders of frequency variation from 10¹ to 10⁶ Hz.

3.8 Dependence of σ_{dc} on τ_s and X_c

Figure 8 presents the variation of σ_{dc} , τ_s , and X_c with x wt% of TiO_2 for these NSPE films at 27 °C, which are considered here to examine the dependence of σ_{dc} values on the τ_s and X_c values of these materials. It can be noted from this figure that the $X_{c(t)}$ of these NSPE films irregularly increase with the increase of TiO_2 content, whereas $X_{c(p)}$ decreases anomalously. The σ_{dc} values of these NSPEs up to 15 wt%

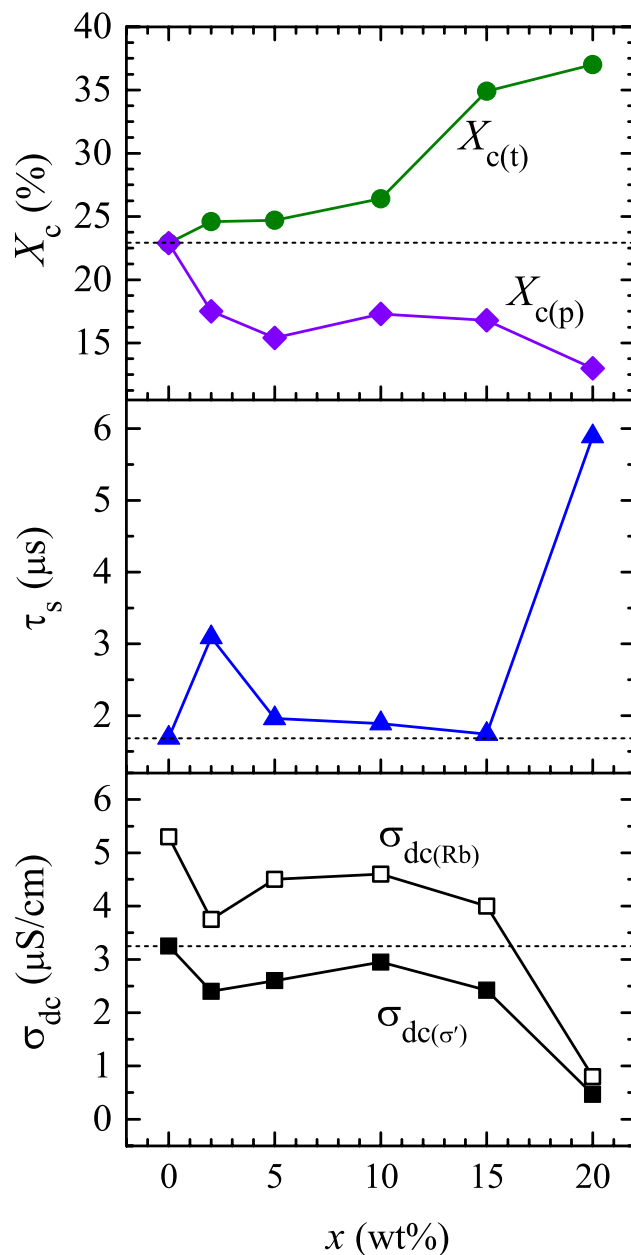


Fig. 8 Degree of crystallinity X_c (%) ($X_{c(p)}$ and $X_{c(t)}$), chain segmental relaxation time τ_s , and dc ionic conductivity σ_{dc} ($\sigma_{dc(\sigma')}$ and $\sigma_{dc(\text{Rb})}$) versus x (wt%) plots of (75PEO/25PVDF)/2 wt% LiClO_4 - x wt% TiO_2 films ($x=0, 2, 5, 10, 15$, and 20), at 27 °C

TiO_2 concentration are found slightly low as compared to NSPE0 film without nanofiller but the conductivity is decreased by about one order of magnitude for 20 wt% TiO_2 containing NSPE20 film. If only the NSPE0 and NSPE20 films are considered, then from their results it can be firmly concluded that the increase of $X_{c(t)}$ reduces the σ_{dc} , but this fact is not found true for the NSPEs having TiO_2 contents in the range 2–15 wt%. However, if the effect of $X_{c(p)}$ is taken into account, then the σ_{dc} values of all the NSPE films must be high as compared to NSPE0 film without nanofiller because of their low $X_{c(p)}$ values. But this fact is also found invalid for all these electrolyte materials. Therefore, it cannot be concluded that only the degree of crystallinity (either of the host polymer matrix or the bulk composite electrolyte material) governs the ionic conductivity of such heterogeneous electrolyte materials.

The τ_s values are found a little higher for the NSPEs as compared to that of the NSPE0 film, and therefore it can be concluded that the increase of τ_s reduces the σ_{dc} values. For 20 wt% TiO_2 containing NSPE20 film, its τ_s is about half order high and the σ_{dc} is low by the same amount. For all these NSPE materials, an almost inverse relationship between the σ_{dc} and τ_s values can be noted from Fig. 8. This fact establishes that the ion transportation is predominantly ruled by the relaxation time of ions coupled polymer chain segmental motion in these heterogeneous ion-dipole-nanofiller networks. This finding is in good agreement with the results on several other types of solid polymer electrolytes characterized by employing the DRS technique [20, 26, 27, 29, 31–33, 69, 70]. The comparison of σ_{dc} , τ_s , and X_c values of these different wt% TiO_2 dispersed NSPE films also illustrates that their content of amorphous phase and the relative variation of ion coupled chain segmental dynamics compensate the effect of one another on the σ_{dc} values. For example, 15 wt% TiO_2 containing NSPE15 film has a large increase in $X_{c(t)}$ value and therefore, there must be a huge drop in its σ_{dc} value, but it is not there because the τ_s value of this film is relatively low. Similarly for NSPE20 film, both the X_c and τ_s values are high and thus this film exhibits a relatively low value of σ_{dc} as expected in comparison to that of the lower TiO_2 concentration NSPE films.

3.9 Electrochemical performance

The electrochemical parameters namely working voltage (V_g), electrochemical stability window (ESW), total ion transference number (t_{ion}), and also reversibility performance of these NSPE films were explored from their LSV, CV, and CA traces recorded at 27 °C, and the same are depicted in Fig. 9.

The LSV traces of these NSPE films (Fig. 9a) clearly show that the current is almost zero with sweeping the voltage

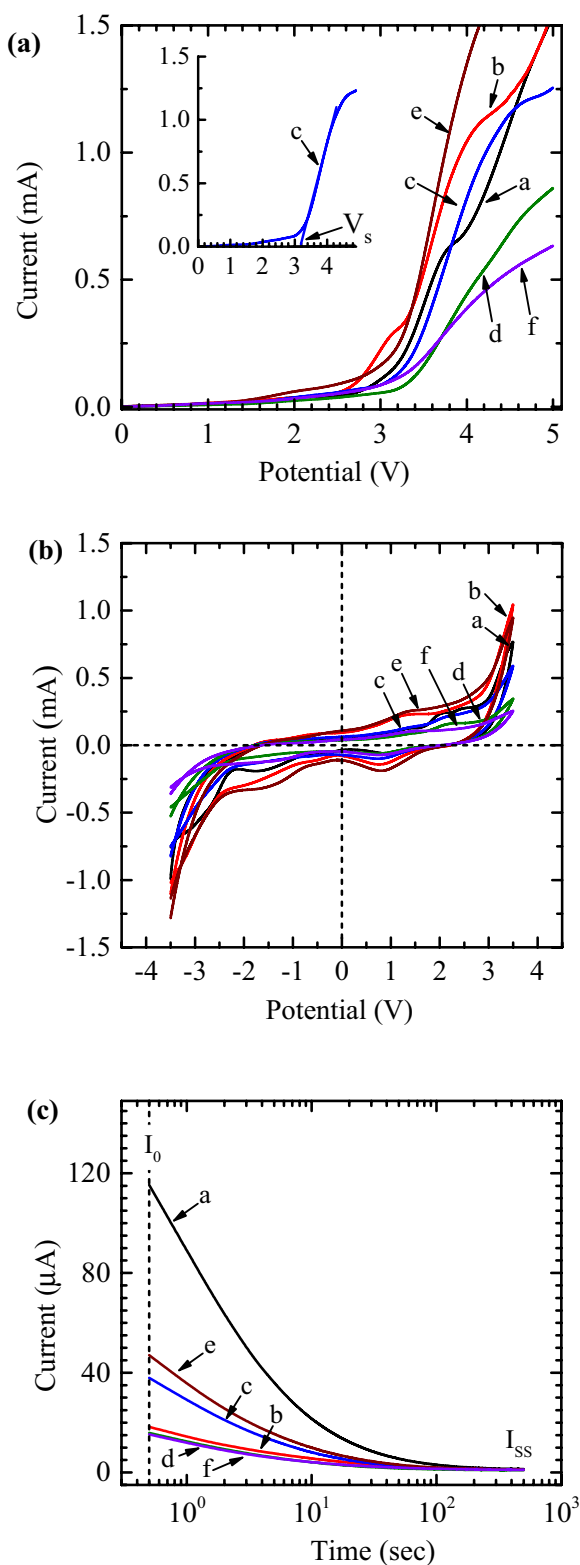


Fig. 9 **a** Linear sweep voltammograms (LSVs), **b** cyclic voltammograms (CVs), and **c** chronoamperograms (CAs) of (75PEO/25PVDF)/25 wt% LiClO₄-*x* wt% TiO₂ films (*x*=0 (a), 2 (b), 5 (c), 10 (d), 15 (e), and 20 (f)), at 27 °C

from zero to about 3 V confirming the stability of the materials up to 3 V, and after that, it increases rapidly indicating that some decomposition of the electrolytes have started on the blocking electrodes. The threshold voltage at which decomposition of the material starts is termed as stability voltage (V_s), and for all the studied NSPE films its value is found ≥ 3 V which is a considerable value confirming them as potential candidates for the high voltage LIBs [8, 10, 19, 35, 69, 70]. The CV traces of the NSPE films are presented in Fig. 9b which reveals that all these electrolyte films exhibit excellent reversibility performance over the ESW range that is taken equal to $2V_s$.

Figure 9c depicts the CA traces from which it can be noted that the initial current I_0 is comparatively high for the NSPE0 film and it varies anomalously with the increase of TiO₂ concentration in these NSPE films. Further, current in these materials decreases rapidly with the increase of polarization time, and finally approach the steady state I_{ss} . The values of I_0 and I_{ss} noted from CA traces were used for the determination of t_{ion} values for these NSPE films using the relation given in recent publication [70], and the determined values are recorded in Table 2. It can be read from this table that the t_{ion} values of all these NSPE materials are close to unity confirming that the electrical conductivity is predominantly ionic, and therefore these materials can serve as an appropriate ionic conductor between the anode and cathode of a rechargeable solid-state lithium-ion battery [8, 10].

3.10 Effect of TiO₂ on the ionic conductivity of various NSPE films: an overview

Herein, the results of earlier investigations on the ionic conductivity of varying concentration TiO₂ nanoparticles incorporated different polymer matrices based lithium-ion conducting NSPE materials at ambient temperature are summarized for better understanding of the role of TiO₂ nanofiller on the ion transportation. The increase in conductivity by about one and a half order of magnitude (i.e., from 7.1×10^{-7} to 1.2×10^{-5} S/cm) is reported for the (PEO-PVC)-LiPF₆ solid complexes with the loading of 10 wt% TiO₂ [18]. Similarly, it was noted that the ionic conductivity of PEO-LiCF₃SO₃ electrolyte had increased by one order of magnitude with 10 wt% TiO₂ addition (i.e., from 1.4×10^{-6} to 4.9×10^{-5} S/cm) [22]. Recently, in situ synthesized lithium-ion conducting poly(ethylene citrate) with embedded titania nanoparticles yielded a maximum increase of conductivity from 5.92×10^{-6} to 1.74×10^{-4} S/cm for 20 wt% of TiO₂ nanofiller [30]. For the plasticized PMMA-LiClO₄ based NSPE films, a maximum ionic conductivity of 3×10^{-4} S/cm was observed for 1 wt% TiO₂ nanoparticles with respect to 2.53×10^{-6} S/cm for the electrolyte film without nanofiller [53]. The PEO-LiTDI

ion–dipole complexes also exhibited an increase in conductivity by one order of magnitude (i.e., from 2.05×10^{-6} to 2.11×10^{-5} S/cm) with the loading of 8 wt% TiO₂ [57]. One order of magnitude conductivity enhancement that is from 1.27×10^{-6} to 1.20×10^{-5} S/cm was also reported for the PEO–LiClO₄ electrolyte films when 3 wt% TiO₂ nanoparticles were dispersed [58]. A little increase in ionic conductivity from 3.1×10^{-3} to 3.9×10^{-3} S/cm was observed for 3 wt% in situ TiO₂ inclusion for the PVDF/PMMA matrix-based gel polymer electrolytes (GPEs) [60]. The PVA–LiClO₄ complex based NSPE films exhibited anomalous behaviour of ionic conductivity with the increase of TiO₂ nanofiller but the highest value of conductivity was observed for 8 wt% TiO₂ loaded ion–dipole-nanoparticle complexes [61].

In the case of PEO–EMIHSO₄ gel electrolytes, the enhancement of conductivity was observed by a factor of two which is from 0.85×10^{-3} to 1.76×10^{-3} S/cm with the addition of 10 wt% TiO₂ nanofiller [62]. Further, the electrospun nanofibrous composite polymer electrolytes (PEO/LiClO₄/PC/EC/TiO₂) also exhibited the highest ionic conductivity 8.5×10^{-5} S/cm at 0.175 wt% TiO₂ nanofiller [51]. It was also reported that in comparison to the commercial TiO₂ sub-micron as filler, the use of TiO₂ nanorods is more effective in the enhancement of lithium-ion conductivity in the PVDF–HFP based composite polymer electrolytes [55]. The NSPEs based on PMMA/SAN/EC/PC/LiCF₃SO₃ complexes dispersed with 9 wt% anatase-TiO₂ nanofiller exhibited high ionic conductivity (1.05×10^{-4} S/cm) which is not because of the TiO₂ filler alone but also due to the contribution of EC/PC plasticizer [56]. The EC/DEC plasticized PVDF/PVC/LiBOB complexes showed enhanced ionic conductivity up to 5.43×10^{-4} S/cm with 2.5 wt% of TiO₂ nanofiller [76]. It is also noted that there is an enhancement of thermal and electrochemical properties of the PVDF–HFP/PMMA/LiPF₆ electrolyte membrane with the addition of TiO₂ nanoparticles and their ionic conductivity also enhances [77]. The plasticized nanocomposite solid polymer electrolyte membranes based on PEMA/PVAc/LiClO₄/EC/*x* wt% TiO₂ exhibited maximum ionic conductivity of 2.745×10^{-3} S/cm with 10 wt% TiO₂ loading [78]. Although these numerous studies on TiO₂ nanoparticles incorporated NSPE materials claimed that this inorganic nanofiller increases the ionic conductivity of the electrolytes, there is a huge anomaly on the effective concentration of TiO₂ nanofiller in regards to enhancement of ionic conductivity. Therefore, on the basis of above mentioned results, it is difficult to conclude firmly that a particular type of TiO₂ and/or a fixed concentration is actually effective in tailoring the ionic conductivity of the NSPE materials. More recently, the effect of the shape of TiO₂ nanofiller on the ionic conductivity of PEO–LiClO₄

electrolytes has been explored [79]. This study concluded that the improvement of conductivity with 2 wt% TiO₂ nanorods is one order of magnitude higher than that with 5 wt% elliptical TiO₂ and it further explained the shape-property relationship in such NSPE materials.

In contrast to the above results, it was also explained that there is a little impact of the untreated surface TiO₂ nanoparticles on the conductivity of polymeric electrolytes above the polymer melting temperature, but superacidic groups introduced on the nanoparticle surface can significantly increase the ionic conductivity [63]. Similar to these results, another study further revealed that the acidic surface-modified filler is more effective in the enhancement of ionic conductivity of the solid polymer electrolytes [64]. Furthermore, the characterization of TiO₂-grafted nanohybrid polymer electrolytes exhibits superior electrochemical properties with an ionic conductivity of 1.1×10^{-4} S/cm at 30 °C [80]. Similarly, the results of PVA/PVDF/LiCF₃SO₃ electrolytes with TiO₂ filler suggested that the addition of TiO₂ filler slightly enhances the ionic conductivity [81]. Our recent investigation on fixed TiO₂ concentration based plasticized nanocomposites solid polymer electrolytes evidenced that the high concentration of PC plasticizer along with 10 wt% TiO₂ nanofiller slightly enhances the ionic conductivity i.e., by a factor of about two only [69].

But some studies have firmly demonstrated that there is a lowering of ionic conductivity of the solid polymer electrolytes upon the addition of inert inorganic oxide nanofillers [20, 82, 83]. The results of atomistic molecular dynamics simulations performed on PEO–LiBF₄ complexes with TiO₂ and Al₂O₃ nanoparticles proved that the segmental dynamics becomes retarded with the addition of inorganic nanofiller near the surface of nanoparticles and also disrupt the polymer conformation resulting a huge decrease of ions mobility and therefore the ionic conductivity of these composite electrolyte [65, 66, 84]. The recent results on coin cell employed NSPE film of PVDF–HFP/LiBOB/TiO₂ (72:18:10 wt%) also confirmed that the ionic conductivity slightly decreased (1.27×10^{-6} S/cm) as compared to that of the PVDF–HFP/LiBOB electrolyte without nanofiller (2.02×10^{-6} S/cm) [85]. The results of the present study on the ionic conductivity of (PEO/PVDF)/LiClO₄-*x* wt% TiO₂ films are also found in good agreement with those reported without nanofiller because the decrease in σ_{dc} with the addition of untreated surface TiO₂ nanoparticles is insignificant up to 15 wt% loading. Further, the correlation of σ_{dc} with the chain segmental dynamics which mainly governs the mobility of ions reasonably supported several facts as explained in regards to variation in ionic conductivity with the addition of TiO₂ nanoparticles and other inorganic nanofillers as summarized for all the above mentioned studies [20, 63–66, 80–84].

4 Conclusions

Various NSPE films of (75PEO/25PVDF)/25 wt% LiClO₄-x wt% TiO₂ compositions were prepared by casting from solution. The effect of TiO₂ nanofiller concentration on the morphological, structural, dielectric polarization and relaxation, ionic conduction, and electrochemical properties of these NSPE films was investigated. The XRD results of these electrolytes confirm the presence of a small amount of characteristic PEO crystallites and the β-phase crystals of PVDF, and also unveil significant alteration in these polymers crystals with the addition of TiO₂ nanoparticles. The degree of crystallinity of the blend polymer matrix significantly decreased and that of the bulk composite materials increased in the presence of TiO₂ nanoparticles. The homogeneous dispersion of the TiO₂ nanoparticles is evidenced from the increase in intensities of the characteristic TiO₂ peaks with the increase in its amount in these nanocomposite electrolytes. Further, the morphology of these NSPE films drastically changes with the initial addition of TiO₂ nanoparticles and with the further increase of its concentration.

The dielectric spectroscopic results confirm that these heterogeneous dielectric materials have a dominant contribution of electrode polarization at lower frequencies, interfacial polarization at intermediate frequencies, and molecular and ionic polarization at high frequencies in the frequency range of 20 Hz–1 MHz at 27 °C. The relaxation processes corresponding to these polarizations have been demonstrated by the ‘master curve representation’ of the complex dielectric and electric spectra, simultaneously. The real part of ac electrical conductivity of these NSPE films obeys Jonscher power law in the high frequency region with fractional exponent values ≈ 0.50 to 0.73 confirming that the transport of ions occurs through hopping and the chain segmental dynamics facilitate this mechanism.

The σ_{dc} values thus obtained are found maximum for the NSPEO film without nanofiller, whereas the dispersion of 2 to 15 wt% TiO₂ has led to a small decrease in the ionic conductivity. Further, about one order of magnitude drop in the ionic conductivity value has been observed for the 20 wt% TiO₂ containing NSPE20 film. The comparative results on conductivity and relaxation time unveil the adverse effect of TiO₂ nanoparticles addition on the ion conduction in these PEO/PVDF blend matrix-based NSPE materials. The electrochemical performance of all these NSPE materials is found appreciable regarding their suitability in the development of all-solid-state ion-conducting devices.

Acknowledgements One of the authors (RJS) is indebted to the Department of Science and Technology (DST), New Delhi, for

providing experimental facilities through the DST–FIST program project No. SR/FST/PSI-134/2008, and also to the Government of Rajasthan, Jaipur, through Rashtriya Uchcharat Shiksha Abhiyan (RUSA) grant No. F30(16)SPD/RUSA/2016/218. The author (PD) appreciatively acknowledges the award of Post Doctoral Fellowship (File No. 09/098 (0133)18 EMR–I) by the Council of Scientific and Industrial Research (CSIR), New Delhi.

Compliance with ethical standards

Conflict of interest The authors declare that they have no conflict of interest.

References

- Zhang H, Armand M, Rojo T (2019) Review—innovative polymeric materials for better rechargeable batteries: strategies from CIC Energigune. *J Electrochem Soc* 166:A679–A686
- Yue L, Ma J, Zhang J, Zhao J, Dong S, Liu Z, Cui G, Chen L (2016) All solid-state polymer electrolytes for high-performance lithium ion batteries. *Energy Storage Mater* 5:139–164
- Zhang Q, Liu K, Ding F, Liu X (2017) Recent advances in solid polymer electrolytes for lithium batteries. *Nano Res* 10:4139–4174
- Kalhoff J, Eshetu GG, Bresser D, Passerini S (2015) Safer electrolytes for lithium-ion batteries: state of the art and perspectives. *Chemsuschem* 8:2154–2175
- Xue Z, He D, Xie X (2015) Poly(ethylene oxide)-based electrolytes for lithium-ion batteries. *J Mater Chem A* 3:19218–19253
- Ngai KS, Ramesh S, Ramesh K, Juan JC (2016) A review of polymer electrolytes: fundamental, approaches and applications. *Ionics* 22:1259–1279
- Gracia I, Armand M, Shanmukaraj D (2019) Li metal polymer batteries. In: Murugan R, Weppner W (eds) *Solid electrolytes for advanced applications*. Springer, Cham
- Arya A, Sharma AL (2017) Insights into the use of polyethylene oxide in energy storage/conversion devices: a critical review. *J Phys D: Appl Phys* 50:443002
- He T, Jing M, Yang H, Chen H, Hua S, Ju B, Zhou Q, Tu F, Shen X, Qin S (2019) Effects of gelation behavior of PPC-based electrolyte on electrochemical performance of solid state lithium battery. *SN Appl Sci* 1:205
- Winie T, Arof AK, Thomas S (2020) *Polymer electrolyte: characterization techniques and energy applications*. Wiley-VCH Verlag GmbH & Co KGaA, Weinheim
- Aldalur I, Matinez-Ibañez M, Krztoń-Maziopa A, Piszcz M, Armand M, Zhang H (2019) Flowable polymer electrolytes for lithium metal batteries. *J Power Sources* 423:218–226
- Kisliuk A, Bocharova V, Popov I, Gainaru C, Sokolov AP (2019) Fundamental parameters governing ion conductivity in polymer electrolytes. *Electrochim Acta* 299:191–196
- Monaca AL, Giorgio FD, Focarete ML, Fabiani D, Zaccaria M, Arbizzani C (2017) Polyvinylidene difluoride–polyethyleneoxide blends for electrospun separators in Li-ion batteries. *J Electrochem Soc* 164:A6431–A6439
- Patla SK, Ray R, Asokan K, Karmakar S (2018) Investigation of ionic conduction in PEO–PVDF based blend polymer electrolytes. *J Appl Phys* 123:125102
- Elashmawi IS, Elsayed NH, Altalhi FA (2014) The changes of spectroscopic, thermal and electrical properties of PVDF/PEO containing lithium nanoparticles. *J Alloys Compd* 617:877–883
- Deng F, Wang X, He D, Hu J, Gong C, Ye YS, Xie X, Xue Z (2015) Microporous polymer electrolyte based on PVDF/PEO star polymer blends for lithium ion batteries. *J Membr Sci* 491:82–89

17. Wang X, Hao X, Hengjing Z, Xia X, Tu J (2020) 3D ultraviolet polymerized electrolyte based on PEO modified PVDF-HFP electrospun membrane for high-performance lithium-sulfur batteries. *Electrochim Acta* 329:135108
18. Arya A, Sadiq M, Sharma AL (2018) Effect of variation of different nanofillers on structural, electrical, dielectric, and transport properties of blend polymer nanocomposites. *Ionics* 24:2295–2319
19. Arya A, Sharma AL (2019) Temperature and salt-dependent dielectric properties of blend solid polymer electrolyte complexed with LiBOB. *Macromol Res* 27:334–345
20. Choudhary S, Sengwa RJ (2017) Effects of different inorganic nanoparticles on the structural, dielectric and ion transportation properties of polymers blend based nanocomposite solid polymer electrolytes. *Electrochim Acta* 247:924–941
21. Dhatarwal P, Choudhary S, Sengwa RJ (2018) Electrochemical performance of Li⁺-ion conducting solid polymer electrolytes based on PEO–PMMA blend matrix incorporated with various inorganic nanoparticles for the lithium ion batteries. *Compos Commun* 10:11–17
22. Vignarooban K, Dissanayake MAK, Albinsson I, Mellander BE (2014) Effect of TiO₂ nano-filler and EC plasticizer on electrical and thermal properties of poly(ethylene oxide) (PEO) based solid polymer electrolytes. *Solid State Ionics* 266:25–28
23. Wang YJ, Kim D (2007) Crystallinity, morphology, mechanical properties and conductivity study of in situ formed PVDF/LiClO₄/TiO₂ nanocomposite polymer electrolytes. *Electrochim Acta* 52:3181–3189
24. Mejia A, Devaraj S, Guzmán J, del Amo JML, García N, Rojo T, Armand M, Tiemblo P (2016) Scalable plasticized polymer electrolytes reinforced with surface-modified sepiolite fillers – A feasibility study in lithium metal polymer batteries. *J Power Sources* 306:772–778
25. Duan H, Yin YX, Zeng XX, Li JY, Shi JL, Shi Y, Wen R, Guo YG, Wan LJ (2018) In-situ plasticized polymer electrolyte with double-network for flexible solid-state lithium-metal batteries. *Energy Storage Mater* 10:85–91
26. Dhatarwal P, Sengwa RJ (2017) Effects of PEG plasticizer concentrations and film preparation methods on the structural, dielectric and electrical properties of PEO–PMMA blend based plasticized solid polymer electrolyte films. *Indian J Pure Appl Phys* 55:7–18
27. Das S, Ghosh A (2015) Effect of plasticizers on ionic conductivity and dielectric relaxation of PEO–LiClO₄ polymer electrolyte. *Electrochim Acta* 171:59–65
28. Liu Y, Xu B, Zhang W, Li L, Lin Y, Nan C (2019) Composition modulation and structure design of inorganic-in-polymer composite solid electrolytes for advanced lithium batteries. *Small*. <https://doi.org/10.1002/sml.201902813>
29. Sengwa RJ, Dhatarwal P, Choudhary S (2014) Role of preparation methods on the structural and dielectric properties of plasticized polymer blend electrolytes: Correlation between ionic conductivity and dielectric parameters. *Electrochim Acta* 142:359–370
30. Pignanelli F, Romero M, Castiglioni J, Faccio R, Mombrú AW (2019) Novel synergistic in situ synthesis of lithium-ion poly(ethylene citrate)-TiO₂ nanocomposites as promising fluorine-free solid polymer electrolytes for lithium batteries. *J Phys Chem Solids* 135:109082
31. Sengwa RJ, Dhatarwal P, Choudhary S (2015) Effects of plasticizer and nanofiller on the dielectric dispersion and relaxation behaviour of polymer blend based solid polymer electrolytes. *Curr Appl Phys* 15:135–143
32. Dhatarwal P, Sengwa RJ (2018) Influence of solid polymer electrolyte preparation methods on the performance of (PEO–PMMA)–LiBF₄ films for lithium-ion battery applications. *Polym Bull* 75:5645–5666
33. Choudhary S, Sengwa RJ (2013) Effects of preparation methods on structure, ionic conductivity and dielectric relaxation of solid polymeric electrolytes. *Mater Chem Phys* 142:172–181
34. Prasanth R, Shubha N, Hng HH, Srinivasan M (2014) Effect of poly(ethylene oxide) on ionic conductivity and electrochemical properties of poly(vinylidene fluoride) based polymer gel electrolytes prepared by electrospinning for lithium ion batteries. *J Power Sources* 245:283–291
35. Dhatarwal P, Sengwa RJ (2019) Synergistic effects of salt concentration and polymer blend composition on the crystal phases, dielectric relaxation, and ion conduction in PVDF/PEO/LiCF₃SO₃ solid polymer electrolytes. *Ionics*. <https://doi.org/10.1007/s11581-019-03337-2>
36. Jacob MME, Prabakaran SRS, Radhakrishna S (1997) Effect of PEO addition on the electrolytic and thermal properties of PVDF–LiClO₄ polymer electrolytes. *Solid State Ion* 104:267–276
37. Yang K, Chi Q, Wang X, Jiang Y, Li F, Xue B (2019) The role of halloy site on crystallinity, ion conductivity, thermal and mechanical properties of poly(ethylene-oxide)/halloysite nanocomposites. *J Polym Res* 26:138
38. Hasan N, Pulst M, Samiullah MH, Kressler J (2019) Comparison of Li⁺-ion conductivity in linear and crosslinked poly(ethylene oxide). *J Polym Sci: Part B* 57:21–28
39. Dhatarwal P, Sengwa RJ, Choudhary S (2019) Effectively improved ionic conductivity of montmorillonite clay nanoplatelets incorporated nanocomposite solid polymer electrolytes for lithium ion-conducting devices. *SN Appl Sci* 1:112
40. Utpalla P, Sharma SK, Sudarshan K, Sahu M, Pujari PK (2019) Investigation of the free volume characteristics of PEO based solid state polymer electrolyte by means of positron annihilation spectroscopy. *Solid State Ion* 339:114990
41. Singh MD, Dalvi A, Phase DM, Kumar Y (2020) Li_{1.3}Al_{0.3}Ti_{1.7}(PO₄)₃ reinforced hybrid polymer composites: assessment of enhanced Li⁺ ion transport and potential for solid-state supercapacitor applications. *J Mater Sci* 55:3951–3963
42. Dhatarwal P, Sengwa RJ (2019) Polymers compositional ratio dependent morphology, crystallinity, dielectric dispersion, structural dynamics, and electrical conductivity of PVDF/PEO blend films. *Macromol Res* 27:1009–1023
43. Arya A, Sharma AL (2018) Effect of salt concentration on dielectric properties of Li-ion conducting blend polymer electrolytes. *J Mater Sci* 29:17903–17920
44. Martins P, Lopes AC, Lanceros-Mendez S (2014) Electroactive phases of poly(vinylidene fluoride): determination, processing and applications. *Prog Polym Sci* 39:683–706
45. Lee YY, Liu YL (2017) Crosslinked electrospun poly(vinylidene difluoride) fiber mat as a matrix of gel polymer electrolyte for fast-charging lithium-ion battery. *Electrochim Acta* 258:1329–1335
46. Wang F, Li L, Yang X, You J, Xu Y, Wang H, Ma Y, Gao G (2018) Influence of additives in a PVDF-based solid polymer electrolyte on conductivity and Li-ion battery performance. *Sustain Energy Fuels* 2:492–498
47. Barbosa JC, Dias JP, Lanceros-Méndez S, Costa CM (2018) Recent advances in poly(vinylidene fluoride) and its copolymers for lithium-ion battery separators. *Membranes* 8:45
48. Lee L, Park S-J, Kim S (2013) Effect of nano-sized barium titanate addition on PEO/PVDF blend-based composite polymer electrolytes. *Solid State Ion* 234:19–24
49. Han H, Liu W, Zhang J, Zhao X-Z (2005) A hybrid poly(ethylene oxide)/ poly(vinylidene fluoride)/TiO₂ nanoparticle solid-state redox electrolyte for dye-sensitized nanocrystalline solar cells. *Adv Funct Mater* 15:1940–1944
50. Xi J, Qiu X, Li J, Tang X, Zhu W, Chen L (2006) PVDF–PEO blends based microporous polymer electrolyte: Effect of PEO on

- pore configurations and ionic conductivity. *J Power Sources* 157:501–506
51. Banitaba SN, Semnani D, Rezaei B, Ensafi AA (2019) Evaluating the electrochemical properties of PEO-based nanofibrous electrolytes incorporated with TiO₂ nanofiller applicable in lithium-ion batteries. *Polym Adv Tech* 30:1234–1242
 52. Chen P, Liang X, Wang J, Zhang D, Yang S, Wu W, Zhang W, Fan X, Zhang D (2017) PEO/PVDF-based gel polymer electrolyte by incorporating nano-TiO₂ for electrochromic glass. *J Sol-Gel Technol* 81:850–858
 53. Pal P, Ghosh A (2018) Influence of TiO₂ nano-particles on charge carrier transport and cell performance of PMMA–LiClO₄ based nano-composite electrolytes. *Electrochim Acta* 260:157–167
 54. Arya A, Saykar NG, Sharma AL (2019) Impact of shape (nanofiller vs. nanorod) of TiO₂ nanoparticle on free-standing solid polymeric separator for energy storage/conversion devices. *J Appl Polym Sci* 136:47361
 55. Kumar PS, Sakunthala A, Govindan K, Reddy MV, Prabu M (2016) Single crystalline TiO₂ nanorods as effective fillers for lithium ion conducting PVDF-HFP based composite polymer electrolytes. *RSC Adv* 6:91711–91719
 56. Ganesan SV, Mothilal KK, Selvasekarapandian S, Ganesan TK (2018) The effect of titanium dioxide nano-filler on the conductivity, morphology and thermal stability of poly(methyl methacrylate)—poly(styrene-co-acrylonitrile) based composite solid polymer electrolytes. *J Mater Sci* 29:8089–8099
 57. Polu AR, Rhee H-W (2016) Effect of TiO₂ nanoparticles on structural, thermal, mechanical and ionic conductivity studies of PEO₁₂–LiTfDI solid polymer electrolyte. *J Ind Eng Chem* 37:347–353
 58. Zha J-W, Huang N, He KQ, Dang Z-M, Shi C-Y, Li RK (2017) Electrospun poly(ethylene oxide) nanofibrous composites with enhanced ionic conductivity as flexible solid polymer electrolytes. *High Volt* 2:25–31
 59. Liu Y, Lee JY, Hong L (2003) Morphology, crystallinity, and electrochemical properties of *in situ* formed poly(ethylene oxide)/TiO₂ nanocomposite polymer electrolytes. *J Appl Polym Sci* 89:2815–2822
 60. Zhou L, Wu N, Cao Q, Jing B, Wang X, Wang Q, Kuang H (2013) A novel electrospun PVDF/PMMA gel polymer electrolyte with *in situ* TiO₂ for Li-ion batteries. *Solid State Ion* 249–250:93–97
 61. Lim C-S, Teoh KH, Liew C-W, Ramesh S (2014) Capacitive behavior studies on electrical double layer capacitor using poly(vinyl alcohol)–lithium perchlorate based polymer electrolyte incorporated with TiO₂. *Mater Chem Phys* 143:661–667
 62. Ketabi S, Lian K (2015) The effects of SiO₂ and TiO₂ nanofillers on structural and electrochemical properties of poly(ethylene oxide)–EMIHSO₄ electrolytes. *Electrochim Acta* 154:404–412
 63. Syzdek J, Borkowska R, Perzyna K, Tarascon JM, Wiecek W (2007) Novel composite polymeric electrolytes with surface-modified inorganic fillers. *J Power Sources* 173:712–720
 64. Ganapatibhotla LVNR, Maranas JK (2014) Interplay of surface chemistry and ion content in nanoparticle-filled solid polymer electrolytes. *Macromolecules* 47:3625–3634
 65. Hanson B, Pryamitsyn V, Ganesan V (2013) Mechanisms underlying ionic mobilities in nanocomposite polymer electrolytes. *ACS Macro Lett* 2:1001–1005
 66. Mogurampelly S, Ganesan V (2015) Effect of nanoparticles on ion transport in polymer electrolytes. *Macromolecules* 48:2773–2786
 67. Ganesan S, Balamurugan S, Karthika P, Marimuthu M (2019) Influence of synthesized pyridine and tetra ethylene glycol derivatives in poly(vinylidene fluoride)/poly(ethylene oxide) with Ti coated back contact dye-sensitized solar cells. *Sol Energy* 189:667–684
 68. Dhatarwal P, Sengwa RJ (2019) Impact of PVDF/PEO blend composition on the β-phase crystallization and dielectric properties of silica nanoparticles incorporated polymer nanocomposites. *J Polym Res* 26:196
 69. Dhatarwal P, Sengwa RJ (2020) Dielectric relaxation, Li-ion transport, electrochemical, and structural behaviour of PEO/PVDF/LiClO₄/TiO₂/PC-based plasticized nanocomposite solid polymer electrolyte films. *Compos Commun* 17:182–191
 70. Sengwa RJ, Dhatarwal P (2020) Predominantly chain segmental relaxation dependent ionic conductivity of multiphase semicrystalline PVDF/PEO/LiClO₄ solid polymer electrolytes. *Electrochim Acta* 338:135890
 71. Sengwa RJ, Dhatarwal P, Choudhary S (2018) Study of time-ageing effect on the ionic conduction and structural dynamics in solid polymer electrolytes by dielectric relaxation spectroscopy. *Solid State Ion* 324:247–259
 72. Xu P, Fu W, Cui Z, Ding Y (2018) Enhancement of polar phase and conductivity relaxation in PIL-modified GO/PVDF composites. *Appl Phys Lett* 112:063904
 73. Sengwa RJ, Choudhary S, Dhatarwal P (2019) Nonlinear optical and dielectric properties of TiO₂ nanoparticles incorporated PEO/PVP blend matrix based multifunctional polymer nanocomposites. *J Mater Sci* 30:12275–12294
 74. Sengwa RJ, Choudhary S (2014) Dielectric properties and fluctuating relaxation processes of poly(methyl methacrylate) based polymeric nanocomposite electrolytes. *J Phys Chem Solids* 75:765–774
 75. Choudhary S, Dhatarwal P, Sengwa RJ (2019) Probing the dielectric relaxation processes and their correlation with ions transportation in the complexes of plasticized nanocomposite solid polymer electrolyte. *Indian J Phys* 93:1545–1558
 76. Aravindam V, Vickraman P (2007) Effects of TiO₂ and ZrO₂ nanofillers in LiBOB based PVDF/PVC composite polymer electrolytes (CPE). *J Phys D* 40:6754
 77. Song DY, Xu C, Chen YF, He JR, Zhao Y, Li PJ, Lin W, Fu F (2015) Enhanced thermal and electrochemical properties of PVDF-HFP/PMMA polymer electrolyte by TiO₂ nanoparticles. *Solid State Ion* 282:31–36
 78. Premila R, Subbu C, Rajendran S, Selva kumar K, (2018) Experimental investigation of nano filler TiO₂ doped composite polymerelectrolytes for lithium ion batteries. *Appl Surf Sci* 449:426–434
 79. Vasudevan S, Fullerton-Shirey SK (2019) Effect of nanoparticle shape on the electrical and thermal properties of solid polymer electrolytes. *J Phys Chem C* 123:10720–10726
 80. Ma C, Zhang J, Xu M, Xia Q, Liu J, Zhao S, Chen L, Pan A, Ivey DG, Wei W (2016) Cross-linked branching nanohybrid polymer electrolyte with monodispersed TiO₂ nanoparticles for high performance lithium-ion batteries. *J Power Sources* 317:103–111
 81. Hema M, Tamilselvi P (2016) Lithium ion conducting PVA:PVDF polymer electrolytes doped with nano SiO₂ and TiO₂ filler. *J Phys Chem Solids* 96–97:42–48
 82. Johansson P, Ratner MA, Shriver DF (2001) The Influence of inert oxide fillers on poly(ethylene oxide) and amorphous poly(ethylene oxide) based polymer electrolytes[†]. *J Phys Chem B* 105:9016–9021
 83. Walls HJ, Zhou J, Yerian JA, Fedkiw PS, Khan SA, Stowe MK, Baker GL (2000) Fumed silica-based composite polymer electrolytes: synthesis, rheology, and electrochemistry. *J Power Sources* 89:156–162
 84. Mogurampelly S, Ganesan V (2016) Influence of nanoparticle surface chemistry on ion transport in polymer nanocomposite electrolytes. *Solid State Ion* 286:57–65
 85. Sabrina Q, Sohib A, Lestariningsih T, Ratri CR (2019) The effect of (TiO₂ and SiO₂) nano-filler on solid polymer electrolyte based LiBOB. *J Phys Conf Series* 1191:012028

Publisher's Note Springer Nature remains neutral with regard to jurisdictional claims in published maps and institutional affiliations.